

Dynamic Neural Potential Field: Online Trajectory Optimization in the Presence of Moving Obstacles

Aleksei Staroverov^{1,2}, Muhammad Alhaddad², Aditya Narendra²,

Konstantin Mironov³, Aleksandr Panov^{1,2}

¹Artificial Intelligence Research Institute,

²Moscow Institute of Physics and Technology,

³Ufa University of Science and Technology

staroverov.av@phystech.edu

Abstract:

Generalist robot policies must operate safely and reliably in everyday human environments such as homes, offices, and warehouses, where people and objects move unpredictably. We present Dynamic Neural Potential Field (NPField-GPT), a learning-enhanced model predictive control (MPC) framework that couples classical optimization with a Transformer-based predictor of footprint-aware repulsive potentials. Given an occupancy sub-map, robot footprint, and optional dynamic-obstacle cues, our autoregressive NPField-GPT head forecasts a horizon of differentiable potentials that are injected into a sequential quadratic MPC program via L4CasADi, yielding real-time, constraint-aware trajectory optimization. We additionally study two baselines: (NPField-D1) static-frame decomposition and (NPField-D2) parallel MLP heads for all steps.

In dynamic indoor scenarios from BenchMR and on a Husky UGV in office corridors, NPField-GPT produces safer, more conservative trajectories under motion changes, while D1/D2 offer lower latency. We also compare with the CIAO* and MPPI baselines. Across methods, the Transformer+MPC synergy preserves the transparency and stability of model-based planning while learning only the part that benefits from data: spatiotemporal collision risk. Code and trained models are available at <https://github.com/CognitiveAISystems/Dynamic-Neural-Potential-Field>.

Keywords: Machine Learning for Robot Control, Collision Avoidance, Nonholonomic Motion Planning

1 Introduction

Mobile robots that act autonomously within human-oriented environments can become significant assistants for humans. They can be applied in offices, shops, homes [1], and medical facilities. Autonomous operation requires methods for planning motion within the environment. Trajectory planning is often executed in two stages: first, a rough global path is generated via search-based [2, 3] or sampling-based [4, 5] methods; second, the global path is turned into a local trajectory under kinodynamic constraints and obstacle avoidance. The second stage is often executed online with a receding horizon strategy. Solutions for receding-horizon trajectory planning may be obtained with model predictive path integral (MPPI) [6, 7] or numerical model predictive control (MPC) [8, 9, 10, 11, 12, 13, 14, 15]. MPPI can work with arbitrary obstacle maps, but it can produce invalid or chattering solutions. Numerical MPC provides fast and stable solutions; however, it requires an analytical representation of collision danger either as a set of constraints [10] or as a cost term

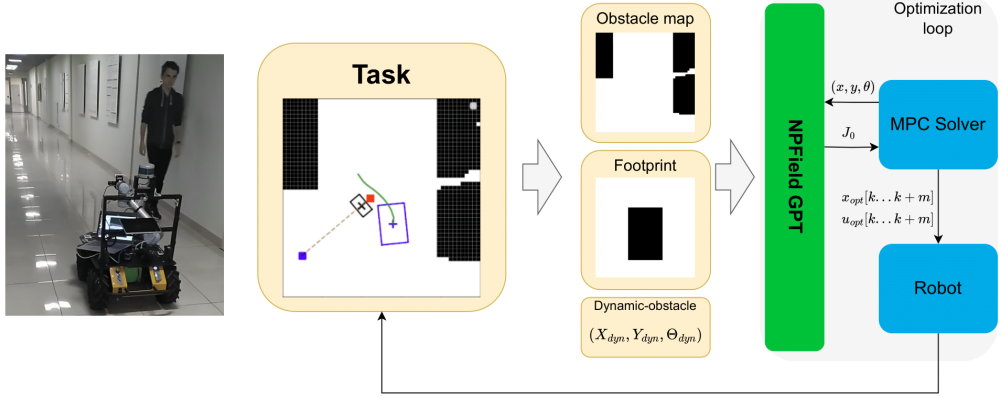


Figure 1: Overview of NPField-GPT integrated with MPC for dynamic obstacle avoidance. Left: Husky UGV operating in an office corridor. Middle: task window with occupancy grid, robot footprint, and a moving obstacle. Right: inputs—obstacle map, footprint, and dynamic-obstacle state $(x_{dyn}, y_{dyn}, \theta_{dyn})$ —are encoded and fed to NPField-GPT to predict a footprint-aware repulsive potential J_o . The potential is consumed inside the optimization loop by the MPC solver to compute $\mathbf{x}_{opt}[k \dots k+m]$ and $\mathbf{u}_{opt}[k \dots k+m]$, which are executed on the robot.

(repulsive potential)¹. In this work, we consider local planning with numerical MPC in the presence of dynamic obstacles (Fig. 1).

Avoiding collisions with dynamic obstacles (e.g., walking human beings in an office environment) is especially challenging. It means that the obstacle map for each frame within the prediction horizon will be different. The prediction of obstacle flow is the specific task [17, 18, 19], which is out of our scope. It may be solved with various methods. Here, we consider dynamic obstacles to be predictable. The dynamic appearance of the obstacle model enlarges the computational complexity of the MPC problem due to a higher number of obstacle parameters.

We argue for a hybrid approach that keeps the strengths of both worlds: learn only the spatiotemporal collision risk, and plan with MPC. Concretely, we extend NPField to dynamic scenes by training a lightweight map/footprint encoder together with a sequence model that predicts a horizon of footprint-aware repulsive potentials. Our primary model (NPField-GPT) is an autoregressive Transformer (GPT) that conditions each step on prior steps, enabling temporally consistent, conservative predictions under motion changes and occlusions. These differentiable potentials are injected into a sequential quadratic program (SQP) for Model Predictive Control (MPC) via L4CasADi, preserving hard-constraint handling and interpretability while benefiting from data-driven risk estimation (Fig. 1).

To study accuracy–latency trade-offs important for deployment, we also consider: (NPField-D1) treating a dynamic scene as a sequence of static frames evaluated step-wise; and (NPField-D2) predicting all steps in parallel with lightweight MLP heads conditioned on dynamic-obstacle cues. Across these variants, we emphasize four workshop-aligned dimensions: Data (learning from occupancy grids plus optional obstacle states), Models (Transformer sequence prediction coupled to MPC), Evaluation (BenchMR scenarios and real Husky trials), and Safety (footprint-aware costs inside a deterministic optimizer).

Our contributions are:

- A Transformer+MPC architecture that forecasts horizon potentials autoregressively and integrates them into real-time, footprint-aware trajectory optimization.

¹The term ”repulsive potential” was introduced for the artificial potential field global planner[16]. In MPC, the trajectory is biased toward safer regions according to the repulsive potential.

- Two complementary baselines (D1/D2) enabling ablations on temporal coupling versus latency.
- An empirical study on dynamic indoor navigation (BenchMR and Husky corridors) showing that NPField-GPT yields safer behavior while D1/D2 minimizes latency, all within real-time budgets.
- Open-source implementation with L4CasADi integration to facilitate reproducible evaluation of learning-in-the-loop planners in everyday environments.

2 Related works

This section discusses existing approaches to motion planning, especially local planning in the presence of moving obstacles and collision avoidance using neural networks. The general planning task consists of finding a trajectory from a given start to a given goal. Well-known global planners such as A* [2], Theta* [3], PRM [4], or RRT [5] generate a reference of intermediate positions of the robot (a global geometric path). Following this reference leads to approaching the destination point. However, in the common case, the geometric path is unaware of how to provide smooth and collision-free motion between intermediate positions. Basic global planners have special extensions, which provide planning with respect to kinodynamic constraints. A* search may be executed on a lattice of kinodynamically feasible motion primitives [20], which results in an executable trajectory instead of a rough geometric path. Motion primitives allow the planner to check that there are no collisions between the intermediate state, including collisions with dynamic obstacles [21, 22, 23, 24]. Sampling-based planners may also be extended to satisfy kinodynamic constraints [25] and replan while avoiding dynamic obstacles [26].

The aforementioned methods aim to add dynamic collision avoidance into the global planning procedure, which might be computationally excessive in case of long global plans and short local horizons. Prediction of dynamic obstacles is often obtained from actual sensor data and requires replanning within a relatively short prediction horizon. Therefore, we further narrow down to receding horizon approaches for local planning.

2.1 Receding horizon planning and dynamic obstacles

The task of local planning is to turn a fixed part of the rough global plan into a smooth trajectory segment under consideration of obstacles and kinodynamic constraints. Model Predictive Path Integral (MPPI) [6] achieves this via sampling random trajectory segments and generating a good solution based on these samples. Collision check for sample trajectories may be systematically extended to the case of dynamic obstacles [27, 28]. Computational heaviness and nondeterministic nature are disadvantages of MPPI; therefore, it may be used in cases when the process model is too complicated for MPC. Numerical MPC solves the local planning task as an optimal control problem. Obstacle avoidance is formalized as a set of constraints (e.g. [10]) or as an additional cost term of the optimization problem. This formalization leads to additional problem parameters describing obstacle properties. The number of parameters should be small to preserve MPC performance. Many approaches approximate the obstacle map with a low-dimensional model. Either obstacles or free space may be approximated with a set of simple geometric figures: points [9], circles [10, 14], rectangles [11], polylines [29], or polygons [8, 30, 15, 31]. Some of these works explicitly consider dynamic environments [29, 30]; others can be adapted straightforwardly (e.g., CIAO* [10, 11] uses independent approximations of the free space at each timestep; these approximations can reflect dynamic obstacles). The limitations of geometric approximations are computational challenges and loss of fidelity. Many works (e.g. [8, 15]) do not consider how to obtain a geometric approximation from an arbitrary obstacle map. In practice, maps are often provided as occupancy grids (a matrix projected onto the map; zero values correspond to free-space cells, while ones correspond to occupied cells). High-resolution grids have too many parameters to be passed to the MPC solver in raw form. In the next subsection, we consider approaches where obstacle data are modeled with neural networks.

2.2 Trajectory optimization with neural collision model

Learning collision model for numeric trajectory optimization was considered in several works [32, 33, 34, 35, 36]. It is challenging to balance the precision and computational complexity of the collision model; therefore, existing works are constrained in terms of computation time and complexity of the maps. [32, 33, 34, 35] use neural models inspired by Neural Radiance Field [37]. These models learn the structure of a single obstacle map (in 2D or 3D) and may be used for navigation within the learned map. [32, 33] exploit network inference for trajectory optimization, while [34, 35] optimize trajectory within the learning procedure. Instead of learning a single obstacle map, the models from [36] take an obstacle representation as input. Both architectures include two submodels: the first reduces the dimensionality of the obstacle representation, while the second calculates the collision score. Therefore, the first submodel provides a compact vector of parameters for a real-time MPC solver, while the second is integrated into this solver using the L4CasADi [33] framework. The difference is that NPField utilizes occupancy grids for footprint-aware collision avoidance of a wheeled mobile robot, while [36] utilizes depth images for 3D collision avoidance of an aerial robot. To our knowledge, there are no neural obstacle models that provide MPC avoidance from dynamic obstacles in real time. [35] exploits a NeRF learning procedure for trajectory optimization in the presence of moving obstacles; however, the computational procedure takes tens of seconds, which is non-real-time. This work aims to provide a model that allows online MPC collision avoidance with a neural model of static and dynamic obstacles.

Positioning and novelty summary. In summary, classical geometric MPC methods (e.g., CIAO* [10, 11]) require handcrafted low-dimensional approximations and do not naturally encode footprint-aware costs from raw grids. Sampling-based methods (MPPI [6, 7]) handle arbitrary maps but can be unstable and slow. Prior neural approaches either learn a single scene [32, 34, 35] or use non-map inputs [36], and most are not designed for real-time optimization in the loop. Our contribution is a family of neural potential field models that: (i) accept occupancy grids and footprint as inputs, (ii) produce differentiable repulsive potentials amenable to real-time MPC via L4CasADi, and (iii) extend to dynamic obstacles through three variants (D1, D2, NPField-GPT) with different accuracy/latency trade-offs.

3 Background

Following NPField, we define the statement and notations for model predictive local planning. We consider a non-holonomic wheeled robot with a differential drive. System state vector $\mathbf{x} = \{x, y, \theta, v\}$ include 2D robot coordinates x and y , its orientation θ and linear velocity v (directed according to θ). Control vector $\mathbf{u} = \{a, \omega\}$ include robot acceleration a (directed according to θ) and angular velocity ω . We consider the model with continuous time dynamics and discrete time control (i.e., u is considered to be constant within the single timestep). A formal statement for the trajectory optimization problem is the following:

$$\{\mathbf{x}_{opt}[i], \mathbf{u}_{opt}[i]\}_{i=k}^{k+m} = \arg \min \sum_{i=k}^{k+m} (\|\mathbf{x}[i] - \mathbf{x}_r[i]\|_{w_x} + \|\mathbf{u}[i]\|_{w_u} + J_o(\mathbf{x}[i], \mathbf{p}_o[i])), \quad (1a)$$

s.t.

$$\frac{dx}{dt} = v \cos \theta, \frac{dy}{dt} = v \sin \theta, \frac{dv}{dt} = a, \frac{d\theta}{dt} = \omega. \quad (1b)$$

Here \mathbf{x}_r is a reference path, \mathbf{p}_o is a vector of obstacle parameters. The total cost function consist of three terms: path following term ($\|\mathbf{x}[i] - \mathbf{x}_r[i]\|_{w_x}$ is a weighted distance between actual trajectory and a reference path), control minimization term ($\|\mathbf{u}[i]\|_{w_u}$ is a weighted norm of the control input), and repulsive potential J_o . Aforementioned statement may be adopted to systems with other dynamic models (e.g., holonomic or car-like robots): this requires the change of \mathbf{x} , \mathbf{u} , and (1b), while the obstacle model will keep the same. Neural potential function is a neural network, which is trained to predict J_o based on \mathbf{x} and \mathbf{p}_o . In NPField \mathbf{p}_o is an embedding of the obstacle map obtained from

the neural encoder. Reference potential for each point is calculated based on signed distance (*SDF*) to obstacle border: $J_o = w_1(\pi/2 + \arctan(w_2 - w_2 SDF))$ (w_1 and w_2 are weighting coefficients). The reference potential for the whole robot is chosen as the maximum potential of the points within its footprint. Reference potential is non-differentiable as *SDF*, and maximum values are calculated algorithmically. Therefore, it cannot be directly used in the MPC loop. Instead, reference potential is used to generate a dataset for training the neural potential field. The difference between static and dynamic environments is that in the first case \mathbf{p}_o is constant for the whole trajectory, while in the second case it depends on time.

Why potentials instead of explicit trajectory prediction? Explicitly predicting obstacle trajectories can provide precise future states but introduces (i) an additional module to train and maintain, (ii) error compounding over the horizon, and (iii) coupling between prediction errors and MPC feasibility. Our approach estimates repulsive potentials that directly shape the MPC cost, offering two key benefits: (a) the optimization remains robust to small prediction inaccuracies because the potential encodes spatial risk rather than a single hypothesized pose, and (b) potentials are differentiable and integrate naturally with L4CasADi for efficient gradient computation. When high-quality motion predictors are available, D1 can consume predicted trajectories in the form of future obstacle maps, while D2/NPField-GPT can be conditioned on predictor states $I_{dyn} = (x, y, \theta)$ and use only the current obstacle map, implicitly extracting information about the dynamic obstacle’s footprint. Thus, our framework complements—rather than replaces—modern predictors by converting them into optimization-friendly costs.

4 Neural Network-Based Potential Field Generation

We study three variants—NPField-D1, D2, and NPField-GPT — for producing footprint-aware repulsive potentials in dynamic scenes. In all cases, a lightweight map/footprint encoder runs once per replan to produce a spatial embedding; at query time, the robot pose and dynamic-obstacle state condition the potential predictor. Full architectural diagrams are shown in Fig. 2. Detailed descriptions of D1/D2 and the auxiliary reconstruction loss are deferred to Appendix C.

Why GPT for dynamic potentials? NPField-GPT replaces independent per-step heads with an autoregressive Transformer that predicts a short horizon of potentials as a sequence. Causal self-attention conditions each step $t+1$ on all prior steps, improving temporal consistency and safety margins relative to one-shot predictions. In our setting, this offers: (i) temporal coherence under motion changes and occlusions; (ii) long-range cross-step conditioning between map features and obstacle motion; (iii) compatibility with MPC via exact differentiation (L4CasADi) and a compact token interface; and (iv) low amortized latency, since the map/footprint encode is computed once and reused.

Concretely, NPField-GPT tokenizes four inputs—map/footprint embedding, robot-conditioned map features, dynamic-obstacle state, and the query pose—and autoregressively emits a length-10 sequence of scalar potentials, one per horizon step. Each new prediction is fed back as a token, enabling consistent, risk-aware forecasts in cluttered corridors.

Baselines. D1 treats a dynamic scene as a sequence of static frames evaluated step-wise; D2 uses parallel MLP heads to predict potentials at all steps from the initial state. These provide strong speed/parameter baselines but lack NPField-GPT’s temporal coupling; see Appendix C.

5 Dataset preparation

We construct a supervised dataset of footprint-aware repulsive potentials on small occupancy-grid crops. Each example consists of: (i) a 50×50 occupancy sub-map at 0.1 m/cell, cropped from MovingAI city maps [38] and an in-house office grid; (ii) the Husky UGV footprint (two variants: folded arm and outstretched arm); (iii) a dynamic obstacle state (0.7×0.5 m rectangle with pose

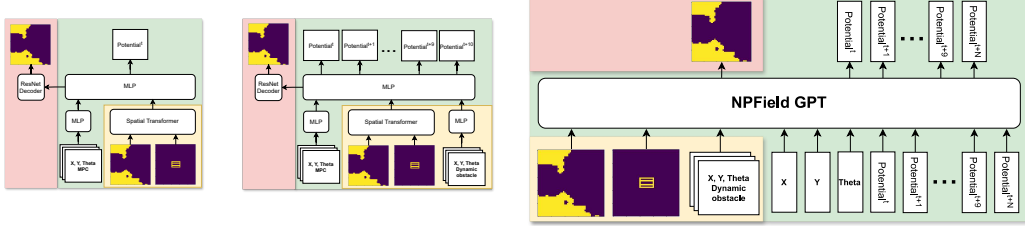


Figure 2: NPField-D1 (left), NPField-D2 (middle), and NPField-GPT (right). Yellow: encoder (map and footprint); green: per-sample potential predictor; red: auxiliary decoder used only for training. D2 uses parallel heads for t_0, \dots, t_{10} , whereas NPField-GPT is an autoregressive transformer-based model that conditions $t+1$ on all prior outputs.

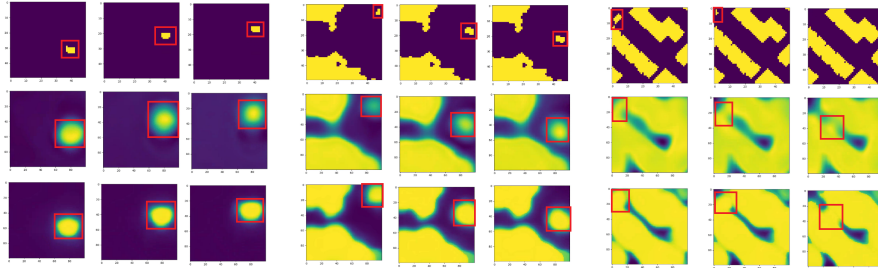


Figure 3: Trajectory predictions for dynamic obstacles generated by NPField-D2 (middle row) and NPField-GPT (bottom row) under three distinct scenarios. Each column corresponds to a scenario, with the first, eighth, and tenth time steps visualized. The models predict repulsive potentials using only the initial map configuration (top row), while subsequent steps are autoregressively generated by NPField-GPT or predicted in parallel by D2 (via MLP heads). The rightmost scenario tests robustness by reversing the dynamic obstacle’s direction (I_{dyn}) relative to the validation dataset. Visualizations depict potentials across the full map for clarity, though the models inherently operate on per-query point-wise predictions.

(x, y, θ) and constant-velocity heading); and (iv) a query robot pose. The target is the footprint-aware repulsive potential computed from the signed distance field as $J_o = w_1(\pi/2 + \arctan(w_2 - w_2 \text{SDF}))$, evaluated as the maximum over cells covered by the footprint. Full generation protocol, dataset counts, and splits are provided in Appendix A.

6 Experiments

Implementation summary. We use Acados (SQP) [39] with CasADI [40] and integrate NPField via L4CasADI [33] for exact differentiation of the neural cost; the stack runs on an AMD Ryzen 5 3500 CPU and an NVIDIA GeForce RTX 2080. End-to-end replanning is typically 0.35–0.70 s across D1,D2,NPField-GPT, dominated by the MPC solve; we pair the local planner with a Theta* [3] global planner. Full implementation, runtime, and scalability details are provided in Appendix B.

6.1 Numerical experiments

We evaluated our algorithm on 100 scenarios (Fig. 4) using the [41] framework, which includes tasks like navigating through narrow passages. The assessment covered standard metrics such as planning time, path length, smoothness, and angle-over-length, where a lower value is preferable for all. Additionally, we introduced a custom metric, ”safety distance” (the minimum value of the SDF).

The experimental results, as detailed in table 1, compared three versions of the Dynamic NPField algorithm: D1, D2, and NPField-GPT, as well as MPPI and the CIAO* [10, 11] trajectory optimiza-

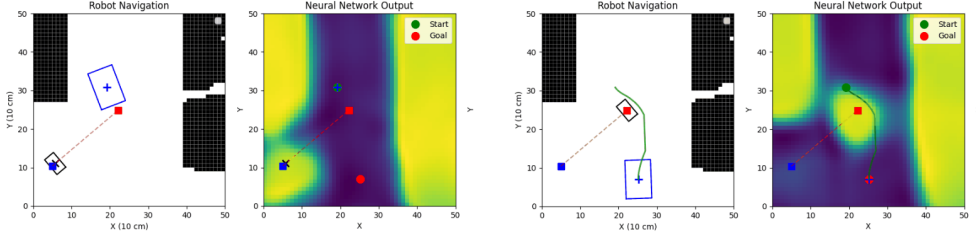


Figure 4: Illustration of a dynamic obstacle navigation scenario using the NPField-GPT architecture. The left panels depict the initial environment (left) and the corresponding neural potential field (right), while the right panels show the final state after trajectory execution. NPField-GPT autonomously predicts obstacle motion based solely on the initial map, without requiring explicit obstacle trajectory inputs, demonstrating self-contained dynamic collision avoidance capabilities.

tion algorithm. As demonstrated in Figure 3, both NPField-D2 and NPField-GPT effectively predict spatiotemporal repulsive potentials for dynamic obstacles. While D2 generates parallel predictions for multiple time steps using MLP heads, GPT employs an autoregressive GPT architecture to sequentially refine potentials, as shown in the eighth and tenth time steps. The rightmost scenario highlights the models’ ability to adapt to abrupt changes in obstacle motion, validating the fidelity of their dynamic embeddings (I_{dyn}).

For each waypoint of the reference CIAO* approximate free space around the robot with a convex figure (circle or rectangle) and constrain the robot to be inside this figure. NPField-D2 and NPField-GPT directly use the data about the bounding box and motion direction of the dynamic obstacle, while NPField-D1 and CIAO* require the projection of the predicted bounding boxes onto the obstacle map.

Overall, CIAO* showed average performance, which aligns with its status as a SOTA method. MPPI had similar results, where it was faster than CIAO* but failed to find optimal trajectories multiple times and overall had sub-par results. NPField-D1 was the fastest, registering a computation time of 359.51 ms, which is nearly 300 ms faster than CIAO*. In contrast, NPField-GPT opted for the shortest path and safest trajectory, as shown by the highest safety distance and lowest AOL, though at the cost of increased computation time and path length. This behavior, although anticipated due to the use of the GPT model, suggests that NPField-GPT might be the most appropriate choice for real-world scenarios where some trade-off in time and length is acceptable to enhance robot safety.

Table 1: Comparative studies on Dynamic obstacles scenarios

Planner	Time, ms	Length, m	Smoothness	AOL	Safety distance, m
MPPI	563.82	4.13	0.036	0.026	0.036
CIAO*	780.83	3.62	0.028	0.019	0.112
NPField-D1	366.62	2.76	0.013	0.033	0.093
NPField-D2	493.50	2.15	0.017	0.058	0.109
NPField-GPT	663.81	2.06	0.011	0.015	0.115

6.2 Real robot experiments

We tested the concept using a Husky UGV mobile manipulator (see Figure 5) as a ROS module. For local planning and control, we utilized MPC, and for global planning, we used the Theta* planner [3]. Our testing scenario involved the robot maneuvering through a complex map. The hardware specifications included an AMD Ryzen 5 3500 CPU and an NVIDIA GeForce RTX 2080 with CUDA support for PyTorch and L4CASADI. The entire navigation stack included a Cartographer and RTAB-Map for the global planner, with a second RTAB-Map for the local planner. All components of the control system were implemented as ROS nodes, with a central node managing



Figure 5: Husky UGV mobile manipulator

communication with the Husky UGV hardware. Real-time planning and execution can be viewed in the supplementary video.

7 Conclusion, limitations and future work

This article presents a novel approach to MPC collision avoidance, which extends Neural Potential Field for the case of an environment with dynamic obstacles. We propose three neural architectures (NPField-D1, NPField-D2, NPField-GPT) for predicting dynamic neural potential. We implement them and compare them with each other and with MPPI and CIAO* trajectory optimizers. NPField-D1 (modeling dynamic environment with a reference to static maps) and NPField-D2 (predicting a reference of potentials at once) outperform CIAO* and MPPI in path length and computation time. NPField-GPT (autoregressive potential prediction) is slower; however, it shows better potential reconstruction in general.

In common, performance measures from table 1 show that our controllers require hundreds of milliseconds to replan the trajectory. This is sufficient for an indoor mobile robot with limited velocity and 1 Hz replanning rate, while faster systems such as cars or drones require a higher rate. Performance may be improved by using more powerful hardware and developing faster models and implementations. Numerical MPC, in general, is sensitive to the quality of the initial guess. In general, it is recommended to use it as a local planner together with a global planner, which provides a rough but suboptimal reference path. Also, it is worth noting that NPField is a learning-based method and therefore it has no theoretical safety guarantees. Therefore, the obtained solution has to be checked for collisions before its execution (which may be easily done by projecting the footprint onto the optimized waypoints).

A significant assumption for the MPC problem is that for each dynamic obstacle, we know either a prediction of its future trajectory (NPField-D1) or a constant direction of its movement. We compensate for the inaccuracy of this assumption via replanning the trajectory on each step. A meaningful direction of future research consists of overcoming this limitation by integrating autoregressive potential forecasting with advanced motion prediction techniques.

References

- [1] A. Szot, A. Clegg, E. Undersander, E. Wijmans, Y. Zhao, J. Turner, N. Maestre, M. Mukadam, D. S. Chaplot, O. Maksymets, et al. Habitat 2.0: Training home assistants to rearrange their habitat. *Advances in Neural Information Processing Systems*, 34:251–266, 2021.
- [2] P. E. Hart, N. J. Nilsson, and B. Raphael. A formal basis for the heuristic determination of minimum cost paths. *IEEE Transactions on Systems Science and Cybernetics*, 4(2):100–107, 1968. [doi:10.1109/TSSC.1968.300136](https://doi.org/10.1109/TSSC.1968.300136).
- [3] A. Nash, K. Daniel, S. Koenig, and A. Felner. Theta^{^*}: Any-angle path planning on grids. In *AAAI*, volume 7, pages 1177–1183, 2007.

[4] L. Kavraki, P. Svestka, J.-C. Latombe, and M. Overmars. Probabilistic roadmaps for path planning in high-dimensional configuration spaces. *IEEE Transactions on Robotics and Automation*, 12(4):566–580, 1996. [doi:10.1109/70.508439](https://doi.org/10.1109/70.508439).

[5] S. M. LaValle and J. James J. Kuffner. Randomized kinodynamic planning. *The International Journal of Robotics Research*, 20(5):378–400, 2001. [doi:10.1177/02783640122067453](https://doi.org/10.1177/02783640122067453).

[6] G. Williams, P. Drews, B. Goldfain, J. M. Rehg, and E. A. Theodorou. Aggressive driving with model predictive path integral control. In *2016 IEEE International Conference on Robotics and Automation (ICRA)*, pages 1433–1440, 2016.

[7] G. Williams, N. Wagener, B. Goldfain, P. Drews, J. M. Rehg, B. Boots, and E. A. Theodorou. Information theoretic mpc for model-based reinforcement learning. In *2017 IEEE International Conference on Robotics and Automation (ICRA)*, pages 1714–1721. IEEE, 2017.

[8] L. Blackmore, M. Ono, and B. C. Williams. Chance-constrained optimal path planning with obstacles. *IEEE Transactions on Robotics*, 27(6):1080–1094, 2011.

[9] J. Ji, A. Khajepour, W. W. Melek, and Y. Huang. Path planning and tracking for vehicle collision avoidance based on model predictive control with multiconstraints. *IEEE Transactions on Vehicular Technology*, 66(2):952–964, 2016.

[10] T. Schoels, L. Palmieri, K. O. Arras, and M. Diehl. An nmpc approach using convex inner approximations for online motion planning with guaranteed collision avoidance. In *2020 IEEE International Conference on Robotics and Automation (ICRA)*, pages 3574–3580, 2020. [doi:10.1109/ICRA40945.2020.9197206](https://doi.org/10.1109/ICRA40945.2020.9197206).

[11] T. Schoels, P. Rutquist, L. Palmieri, A. Zanelli, K. O. Arras, and M. Diehl. Ciao*: Mpc-based safe motion planning in predictable dynamic environments. *IFAC-PapersOnLine*, 53(2): 6555–6562, 2020. ISSN 2405-8963. [doi:<https://doi.org/10.1016/j.ifacol.2020.12.072>](https://doi.org/10.1016/j.ifacol.2020.12.072). URL <https://www.sciencedirect.com/science/article/pii/S2405896320303281>. 21st IFAC World Congress.

[12] Z. Zuo, X. Yang, Z. Li, Y. Wang, Q. Han, L. Wang, and X. Luo. Mpc-based cooperative control strategy of path planning and trajectory tracking for intelligent vehicles. *IEEE Transactions on Intelligent Vehicles*, 6(3):513–522, 2020.

[13] D. Bojadžić, J. Kunze, D. Osmanković, M. Malmir, and A. Knoll. Non-holonomic rrt & mpc: Path and trajectory planning for an autonomous cycle rickshaw. *arXiv preprint arXiv:2103.06141*, 2021.

[14] J. Zeng, B. Zhang, and K. Sreenath. Safety-critical model predictive control with discrete-time control barrier function. In *2021 American Control Conference (ACC)*, pages 3882–3889. IEEE, 2021.

[15] A. Thirugnanam, J. Zeng, and K. Sreenath. Safety-critical control and planning for obstacle avoidance between polytopes with control barrier functions. In *2022 International Conference on Robotics and Automation (ICRA)*, pages 286–292, 2022. [doi:10.1109/ICRA46639.2022.9812334](https://doi.org/10.1109/ICRA46639.2022.9812334).

[16] O. Khatib. Real-time obstacle avoidance for manipulators and mobile robots. In *Proceedings. 1985 IEEE International Conference on Robotics and Automation*, volume 2, pages 500–505, 1985. [doi:10.1109/ROBOT.1985.1087247](https://doi.org/10.1109/ROBOT.1985.1087247).

[17] A. Jain, S. Casas, R. Liao, Y. Xiong, S. Feng, S. Segal, and R. Urtasun. Discrete residual flow for probabilistic pedestrian behavior prediction. In *Conference on Robot Learning*, pages 407–419. PMLR, 2020.

[18] N. Sharma, C. Dhiman, and S. Indu. Pedestrian intention prediction for autonomous vehicles: A comprehensive survey. *Neurocomputing*, 508:120–152, 2022.

[19] Y. Murhij and D. Yudin. Ofmpnet: Deep end-to-end model for occupancy and flow prediction in urban environment. *Neurocomputing*, page 127649, 2024.

[20] J. Butzke, K. Sapkota, K. Prasad, B. MacAllister, and M. Likhachev. State lattice with controllers: Augmenting lattice-based path planning with controller-based motion primitives. In *2014 IEEE/RSJ International Conference on Intelligent Robots and Systems*, pages 258–265. IEEE, 2014.

[21] M. Phillips and M. Likhachev. Sipp: Safe interval path planning for dynamic environments. In *2011 IEEE international conference on robotics and automation*, pages 5628–5635. IEEE, 2011.

[22] J. Lin, T. Zhou, D. Zhu, J. Liu, and M. Q.-H. Meng. Search-based online trajectory planning for car-like robots in highly dynamic environments. In *2021 IEEE International Conference on Robotics and Automation (ICRA)*, pages 8151–8157. IEEE, 2021.

[23] K. S. Yakovlev, A. A. Andreychuk, J. S. Belinskaya, and D. A. Makarov. Safe interval path planning and flatness-based control for navigation of a mobile robot among static and dynamic obstacles. *Automation and Remote Control*, 83(6):903–918, 2022.

[24] Z. A. Ali and K. Yakovlev. Safe interval path planning with kinodynamic constraints. In *Proceedings of the AAAI Conference on Artificial Intelligence*, volume 37, pages 12330–12337, 2023.

[25] L. Palmieri and K. O. Arras. A novel rrt extend function for efficient and smooth mobile robot motion planning. In *2014 IEEE/RSJ International Conference on Intelligent Robots and Systems*, pages 205–211. IEEE, 2014.

[26] M. Otte and E. Frazzoli. Rrtx: Asymptotically optimal single-query sampling-based motion planning with quick replanning. *The International Journal of Robotics Research*, 35(7):797–822, 2016.

[27] I. S. Mohamed, K. Yin, and L. Liu. Autonomous navigation of agvs in unknown cluttered environments: log-mppi control strategy. *IEEE Robotics and Automation Letters*, 7(4):10240–10247, 2022.

[28] S. Patrick and E. Bakolas. Path integral control with rollout clustering and dynamic obstacles. *arXiv preprint arXiv:2403.18066*, 2024.

[29] J. Ziegler, P. Bender, T. Dang, and C. Stiller. Trajectory planning for bertha — a local, continuous method. In *2014 IEEE Intelligent Vehicles Symposium Proceedings*, pages 450–457, 2014. [doi:10.1109/IVS.2014.6856581](https://doi.org/10.1109/IVS.2014.6856581).

[30] G. Franze and W. Lucia. A receding horizon control strategy for autonomous vehicles in dynamic environments. *IEEE Transactions on Control Systems Technology*, 24(2):695–702, 2015.

[31] A. Logunov, M. Alhaddad, K. Mironov, K. Yakovlev, and A. Panov. Polygon decomposition for obstacle representation in motion planning with model predictive control. *Engineering Applications of Artificial Intelligence*, 153:110690, 2025.

[32] M. Adamkiewicz, T. Chen, A. Caccavale, R. Gardner, P. Culbertson, J. Bohg, and M. Schwager. Vision-only robot navigation in a neural radiance world. *IEEE Robotics and Automation Letters*, 7(2):4606–4613, 2022. [doi:10.1109/LRA.2022.3150497](https://doi.org/10.1109/LRA.2022.3150497).

[33] T. Salzmann, J. Arrizabalaga, J. Andersson, M. Pavone, and M. Ryll. Learning for casadi: Data-driven models in numerical optimization. 2023.

[34] M. Kurenkov, A. Potapov, A. Savinykh, E. Yudin, E. Kruzhkov, P. Karpyshev, and D. Tsetserukou. Nfomp: Neural field for optimal motion planner of differential drive robots with nonholonomic constraints. *IEEE Robotics and Automation Letters*, 7(4):10991–10998, 2022. doi:10.1109/LRA.2022.3196886.

[35] M. Katerishich, M. Kurenkov, S. Karaf, A. Nenashev, and D. Tsetserukou. Dnfomp: Dynamic neural field optimal motion planner for navigation of autonomous robots in cluttered environment. In *2023 IEEE International Conference on Systems, Man, and Cybernetics (SMC)*, pages 1984–1989. IEEE, 2023.

[36] M. Jacquet and K. Alexis. N-mpc for deep neural network-based collision avoidance exploiting depth images, 2024.

[37] B. Mildenhall, P. P. Srinivasan, M. Tancik, J. T. Barron, R. Ramamoorthi, and R. Ng. Nerf: Representing scenes as neural radiance fields for view synthesis, 2020.

[38] N. Sturtevant. Benchmarks for grid-based pathfinding. *Transactions on Computational Intelligence and AI in Games*, 4(2):144 – 148, 2012. URL <http://web.cs.du.edu/~sturtevant/papers/benchmarks.pdf>.

[39] R. Verschueren, G. Frison, D. Kouzoupi, J. Frey, N. van Duijkeren, A. Zanelli, B. Novoselnik, T. Albin, R. Quirynen, and M. Diehl. Acados: a modular open-source framework for fast embedded optimal control, 2020.

[40] J. A. E. Andersson, J. Gillis, G. Horn, J. B. Rawlings, and M. Diehl. CasADi – A software framework for nonlinear optimization and optimal control. *Mathematical Programming Computation*, 11(1):1–36, 2019. doi:10.1007/s12532-018-0139-4.

[41] E. Heiden, L. Palmieri, L. Bruns, K. O. Arras, G. S. Sukhatme, and S. Koenig. Bench-mr: A motion planning benchmark for wheeled mobile robots. *IEEE Robotics and Automation Letters*, 6(3):4536–4543, 2021. doi:10.1109/LRA.2021.3068913.

[42] T. Salzmann, E. Kaufmann, J. Arrizabalaga, M. Pavone, D. Scaramuzza, and M. Ryll. Real-time neural mpc: Deep learning model predictive control for quadrotors and agile robotic platforms. *IEEE Robotics and Automation Letters*, 8(4):2397–2404, 2023. doi:10.1109/LRA.2023.3246839.

A Dataset generation details

Maps and crops. We crop large occupancy grids into 50×50 sub-maps at 0.1 m/cell (5×5 m windows), yielding 1000 unique sub-maps for data generation (Fig. 6).

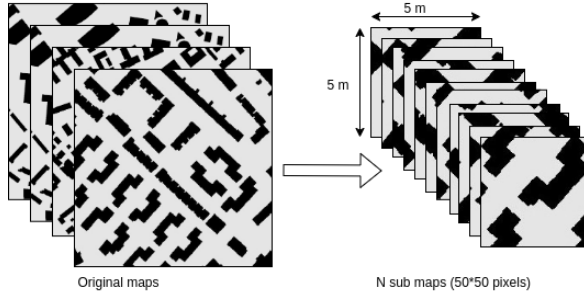


Figure 6: Cropping original maps into sub-maps

Dynamic obstacle placements. For each sub-map, we sample one agent position with three orientations. Assuming 0.3 m/s constant speed, we generate 10 forward positions per orientation (31 variants per sub-map: 1 static-only; 3×10 with the agent).

Reference potentials. For each sub-map copy, we compute the signed distance field (SDF) and derive cell-wise potentials as $J_o = w_1(\pi/2 + \arctan(w_2 - w_2 \text{ SDF}))$. For two Husky UGV footprints (folded and outstretched arm), we evaluate 10 random orientations of the footprint at each query pose and take the maximum over covered cells as the footprint-aware target.

Dataset structure and splits. The dataset is tabular with fields: sub-map ID, query robot pose, dynamic obstacle pose/direction, footprint id, and the target potential. We split by sub-map into train/val/test as 70/15/15%. Validation figures (e.g., Fig. 3) use held-out sub-maps and placements. We also include stress tests by reversing I_{dyn} on validation sub-maps.

B Implementation details, runtime, and scalability

Solver and toolchain. We solve nonlinear MPC with SQP (Acados [39]) and CasADi [40]. We integrate PyTorch NPFIELD models using L4CasADi [33] for exact symbolic differentiation (preferred over ML-CasADi [42], which uses local Taylor approximations).

Neural integration. The map/footprint encoder runs once per replan on GPU; point-wise potential heads (D1/D2) are batched over horizon steps, while NPFIELD-GPT runs autoregressively across time steps.

Runtime breakdown. On AMD Ryzen 5 3500 CPU and NVIDIA RTX 2080: (i) map/footprint preprocessing and h_{map} (GPU) 6–12 ms; (ii) per-sample embedding and NPFIELD forward (GPU) D1: 30–40 ms, D2: 55–80 ms, NPFIELD-GPT: 120–160 ms; (iii) Acados SQP solve with L4CasADi cost (CPU) 250–550 ms; (iv) ROS I/O 10–20 ms.

Scalability. Let N be horizon and M dynamic obstacles. D1: $\mathcal{O}(N)$ single-step calls; D2: $\mathcal{O}(1)$ head depth per step (batched); NPFIELD-GPT: $\mathcal{O}(N)$ autoregression with shared attention. MPC is roughly quadratic in N with dense costs; we use warm starts and structure. For multiple obstacles, we concatenate I_{dyn} and cap M by the nearest obstacles per window.

Planning stack. We pair the local MPC with Theta* [3] for global polylines. Theta* uses a circular footprint for robustness; local MPC enforces footprint-aware safety.

C Architectural details and auxiliary losses

NPField-D1 (static-frame decomposition). A dynamic scene is represented as a sequence of static maps; the potential is evaluated per step with the same spatial encoder. This yields strong latency and simplicity, but temporal consistency is implicit and delegated to the MPC horizon.

NPField-D2 (parallel heads). A single encoder is paired with multiple lightweight MLP heads, one per future step (t_0, \dots, t_{10}), conditioned on the dynamic-obstacle state $I_{dyn} = (x, y, \theta)$. This keeps parameter count low and supports batched prediction, but steps are independent and may drift temporally under distribution shift.

Auxiliary reconstruction loss. During training only, we decode the map embedding back to an occupancy grid with a small CNN head and apply binary cross-entropy over cells. This regularizes the spatial embedding, improving stability for NPField-D2/NPField-GPT without affecting test-time runtime (the decoder is discarded).

D Training hyperparameters and pseudocode

Model hyperparameters (NPField-GPT head).

- Transformer: $d_{model}=864$, $n_{head}=8$, $n_{layer}=6$, dropout 0.1; autoregressive causal mask; MLP output head.
- Map/footprint encoder: hidden channels 64, attention blocks 4, attention heads 4, CNN dropout 0.15, downsample steps 2, input 50×50 .
- Decoder projection: flattened feature size $3456 \rightarrow d_{model}$.
- Outputs: horizon length 10; loss is MSE on normalized potentials.

Optimization.

- Optimizer: Adam, learning rate 1×10^{-4} , gradient clipping at 0.9.

Dataset interface. Each sample contains: (i) stacked map and footprint, (ii) query pose (x, y, θ) , (iii) dynamic obstacle state (x, y, θ) , and (iv) a length-10 potential target sequence for the scenario window.

Training loop (pseudocode).

1. Build dataloaders with the fixed dataset covering all map/pose/head combinations.
2. For each batch: encode map/footprint once; encode query pose and dynamic state; run autoregressive Transformer to predict a length-10 potential sequence.
3. Compute MSE to the target sequence; backprop, clip gradients, step optimizer.

E MPC integration pseudocode

1. Wrap the trained PyTorch potential head with L4CasADI to obtain a differentiable CasADI function that maps $[\text{embedding}, x, y, \theta] \mapsto \text{horizon potentials}$.
2. In the Acados model, define states (x, y, v, θ, t) and controls (a, ω, T) ; pass the embedding as a parameter vector.
3. Inside the cost, call the L4CasADI function, flatten the returned vector, and select the element matching the current time slice.
4. Minimize a nonlinear least-squares objective combining tracking, control effort, and the neural potential term; solve with SQP.